Performance Measurement and Propellant Testing for the STEP-1 CubeSat Elecrospray Thrusters

Performance Measurement and Propellant Testing for the STEP-1 CubeSat Elecrospray Thrusters

IEPC-2022-216

Presented at the 37th International Electric Propulsion Conference
Massachusetts Institute of Technology, Cambridge, MA, USA
June 19-23, 2022

Gustav M. Pettersson[1], Amelia R. Bruno[2], Matthew N. Corrado[3],
Bryan S. Medina[4], David Krejci[5] and Paulo C. Lozano[6]
Massachusetts Institute of Technology, Cambridge, MA 02139

Electrosprays are a promising technology for highly effective propulsion for CubeSats and other small satellites. In this work we present the design, initial operations, and performance measurements of the latest generation of ion Electrospray Propulsion System (iEPS). Choosing the best ionic liquid propellant is discussed, where we note that the common EMI-BF4 tends to absorb large amounts of water from the atmosphere. We suggest instead to use EMI-CF3BF3, which hardly absorbs water and performs as well or better than EMI-BF4 in our results. The thrusters tested here produce around 12 micronewtons of thrust at a specific impulse of around 600 seconds, while only consuming 120 milliwatts of power.

I. Nomenclature

c	=	Effective exhaust velocity
F	=	Thrust
F_{TOF}	=	Uncorrected thrust from TOF
g	=	Acceleration due to gravity, 9.81 m/s^2
I_{em}	=	Emitted current
I_{sp}	=	Specific impulse
$I_{sp,TOF}$	=	Uncorrected specific impulse from TOF
I_{sp}^{ideal}	=	Lossless specific impulse
$I(t)$	=	Current over time at TOF detector
$I(\theta)$	=	Current angular distribution
L_{TOF}	=	Field-free drift length for TOF
$\dot{m}$	=	Mass flow
$\dot{m}_{TOF}$	=	Mass flow measured from TOF
$\mathbb{P}$	=	Electrical power
q/m	=	Charge to mass ratio of emitted ions
t	=	Time
t_{TOF}	=	Time of flight from gate to detector
V_0	=	Thruster firing voltage
V_{RPA}	=	Retarding potential (voltage)
η	=	Overall power efficiency

[1]Ph.D. Candidate, Department of Aeronautics and Astronautics, gupet@mit.edu.
[2]Ph.D. Candidate, Department of Aeronautics and Astronautics, arbruno@mit.edu.
[3]Ph.D. Candidate, Department of Aeronautics and Astronautics, mcorrado@mit.edu.
[4]Undergraduate Student, bmedina@mit.edu.
[5]Now with Enpulsion GmbH, Austria, david.krejci@enpulsion.com.
[6]M. Alemán-Velasco Professor, Department of Aeronautics and Astronautics, plozano@mit.edu.

η_E = Energy efficiency
η_i = Ionisation efficiency
η_p = Polydispersive efficiency
η_{tr} = Transmission efficiency
η_θ = Angular efficiency
θ = Firing angle away from centreline

II. Introduction

Ion-electrospray thrusters are a potential method for providing high Δv propulsion capabilities for small spacecraft and CubeSats. While electrospray (colloid) thrusters were well studied in the 1960s [1], they gained popularity after the discovery of the pure ion evaporation regime [2] and the rise in micropropulsion interest for CubeSats. A variety of other electric propulsion technologies are in development for high Δv CubeSats such as field-emission electric propulsion (FEEP) [3] and radio-frequency (RF) ion thrusters [4] which were recently demonstrated in space. While all systems have their own set of advantages and disadvantages, ion-electrospray systems [5] are characterised by their high power efficiency and compactness. These benefits draw from the "pre-ionised" room-temperature propellant and bipolar operation of electrosprays, which eliminate the energy intensive heaters, ionisation chambers, and neutralising cathodes required by most electric propulsion technologies. The Staged Electrospray Pathfinder 1 (STEP-1) mission is a technology demonstration aiming to further develop and mature ion electrospray propulsion systems.

Several ionic liquids have been electrosprayed in laboratory environments, and propellants based on the 1-ethyl-3-methylimidazolium (EMI) cation, with anions tetrafluoroborate (BF4) [5] or bis(trifluoromethylsulfonyl)imide (Im) [6] have been selected for flight. EMI-BF4 is especially suitable for electrosprays since it operates well in the pure-ion mode, however, it is known to be highly hygroscopic and can gain more than 30% of its mass in water from ambient air [7]. One benefit of ionic liquid electrosprays is that they allow the use of compact and light unpressurised propellant tanks, which means that they are directly subjected to the ambient environment and may absorb significant amounts of water from it. Due to this, we will evaluate two alternative EMI-based ionic liquids, with anions trifluoro(trifluoromethyl)borate (CF3BF3) and dicyanamide (DCA), for use in bipolar electrosprays and measure the water absorption properties of all four propellants.

In this work we further introduce the latest generation ion Electrospray Propulsion System (iEPS) thruster, where the emitter-extractor chip has been updated with new materials and design, and the tank assembly includes a valve to guarantee propellant containment. The thrusters tested here are the three first units built to the STEP-1 specification and includes details on their design, operations, and preliminary performance.

A. Propellant selection

The four propellants to be considered are EMI-BF4, EMI-CF3BF3, EMI-Im, and EMI-DCA. Their basic physical properties are given in Table 1. From a storability perspective we desire a propellant with high density, low hygroscopicity, and a low freezing point, although the latter is not critical for ionic liquids which tend to supercool far below their freezing point [8]. For bipolar operation, a wide electrochemical window (EW) is ideal to avoid reactions in the tank, and a near equal mass of the anion and cation is important for consistent performance. Naturally, we desire a propellant which "electrosprays well", which is an elusive property best determined by experiments, however conductivity and viscosity are thought to be some important macrophysical properties.

Table 1 Ionic liquid physical properties at 25 °C **from [9]. The EMI anion has a mass of** 111.1 Da**.**

Propellant	Cation mass	Density	Freezing point	Conductivity	Viscosity	EW
EMI-BF4	86.8 Da	1.28 g/cm^3	15 °C	1.36 S/m	42 cP	4.55 V
EMI-CF3BF3	136.8 Da	1.35 g/cm^3	−20 °C	1.48 S/m	26 cP	4.63 V
EMI-Im	280.2 Da	1.52 g/cm^3	−15 °C	0.92 S/m	34 cP	4.59 V
EMI-DCA	66.1 Da	1.06 g/cm^3	−21 °C	2.2 S/m	21 cP	3 V

For EMI-Im the cation mass is over 2.5 times the anion mass which makes it unsuited for bipolar operation, despite otherwise having a high density and absorbing little water from the environment (see Section V.E). The mass ratio for EMI-DCA is also relatively large, with a low density. However, the high conductivity and low viscosity suggests it may

operate well in an electrospray thruster. As we show, EMI-DCA absorbs water from the environment quickly, ultimately making it unsuitable for the application. The final candidate, EMI-CF3BF3, has similar physical properties to EMI-BF4 and, as we demonstrate, does not absorb much water. This may thus be a preferable propellant and in this work will will perform a performance comparison between EMI-CF3BF3 and EMI-BF4 to determine the choice for STEP-1.

III. Thruster design

A. Thruster chip

The MIT iEPS thruster chip consists of three layers: the emitter, the extractor, and the frame. An exploded view is shown in Fig. 1a. The emitter is an array of 480 emitter tips laser ablated from a 1×1 cm porous glass substrate. In the latest generation of thrusters, Shirasu Porous Glass by SPG Technology Co. is used as the emitter material. This substrate has highly uniform pore size and is available in various pore sizes as small as 0.1 µm, which gives increased control of the geometry. The extractor is an array of apertures which align with the emitter tips, and is microfabricated from silicon and coated in gold to increase conductivity. For this thruster the extractor grid is 40 µm thick above the emitters and has a chamfered edge to reduce the intercepted current [10]. The emitter is bonded to a structural frame that provides alignment and high voltage isolation between the emitter and extractor. The frame is microfabricated from silicon and bonded to glass to form "posts" at each of the four corners. The posts have a locking geometry to align the extractor layer and the glass enables electrical isolation. Propellant is fed to the back of the porous chip via an opening in the frame. The propellant can then spread easily through the emitter bulk and into the tips.

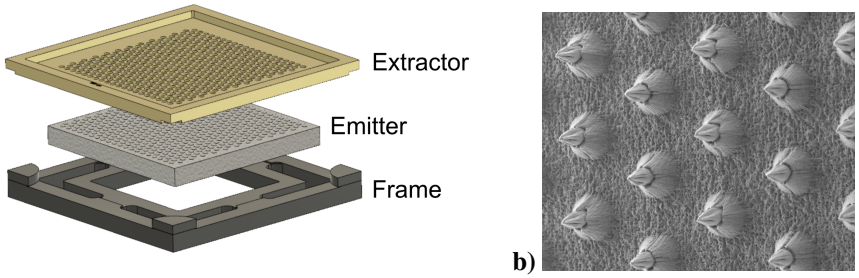

Fig. 1 a) An exploded view of the thruster chip, showing extractor, emitter, and frame. b) Scanning electron microscope image of emitter tips.

B. Thruster tank

The thruster chip is mounted onto a propellant tank assembly for flight, as shown in Fig. 2a. The tank is designed to contain and manage propellant as well as provide an electrical connection to the ionic liquid, which is required to fire the thruster. A cross-sectional schematic of the tank assembly with labelled components is depicted in Fig. 2b. The propellant tank housing is comprised of two nested shells. The inner shell is made of porous PTFE, which allows gases and volatiles to vent directly through the walls while retaining the ionic liquid. The PTFE insert is encased by an outer PEEK shell for mechanical support. A carbon aerogel electrode is embedded into the centre of the tank and serves as the electrical connection to the conductive propellant. The distal electrode configuration prevents electrochemical degradation to the ionic liquid propellant over time [11]. The electrode is wrapped in a glass microfiber wick that allows propellant to passively flow into the back of the emitter chip via capillary action.

Between the tank and the emitter is a key component that controls propellant delivery to the thruster chip: a solid-state electrowetting valve. The valve is designed to seal propellant delivery to the emitter throughout launch to prevent propellant leakage and oversaturation of the emitter before firing begins. The operating principle of the valve is electrowetting, a commonly utilised phenomenon in microfluidics, which states that the contact angle between a liquid and a substrate can be modified through application of an electric potential. The valve is a small silicon chip with an array of etched through-hole channels coated with PTFE. At a 0 V potential between the ionic liquid and the valve, the contact angle between the propellant and PTFE layer is sufficient to prevent wetting and liquid from flowing into the channels, shown in Fig. 3a. The body of the valve is connected to ground, therefore when a voltage is applied to the tank distal electrode the propellant will wet the valve, entering the channels and flowing freely, as in Fig. 3b. After

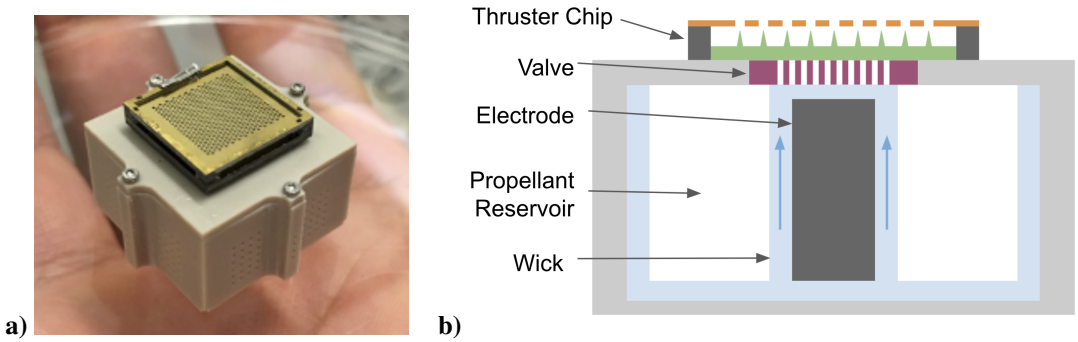

Fig. 2 The iEPS thruster assembly. a) Angled view of a fully assembled iEPS tank with thruster chip mounted on top. b) Cross-section schematic of the thruster tank, with key components labelled.

liquid enters the channel, even if the voltage is removed the fluid path still remains active, depicted in Fig. 3c. The valve ground connection is made through a 1 GΩ resistor to ensure any leakage current is small compared to the emitted current during operations. The valve design and operations were presented in detail in [12].

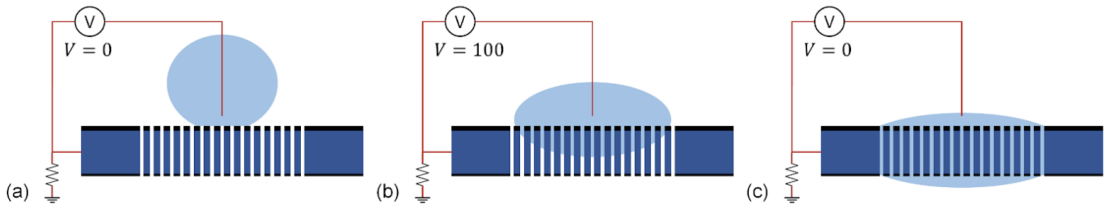

Fig. 3 Operational stages of the electrowetting valve. a) Before activation the propellant is blocked. b) A voltage is applied and electrowetting allows the propellant to enter the channels. c) After the voltage is removed, the fluid path remains once activated.

IV. Methods

A. Thruster operations

For all tests, each thruster was mounted to a circuit board which provides screw terminals for the extractor, emitter (i.e. distal electrode), and valve connections. The board and thruster were covered by a grounded shield during all testing, see Fig. 4a. Operations were performed under high vacuum, below 1 mPa during continuous firing. The thrusters were powered from a Matsusada AP-3B1 high voltage power supply capable of 3 kV and 1 mA output in both positive and negative polarity, with the extractor grounded. Current was measured using a resistor and an Analog Devices AD210AN isolation amplifier for the emitter and extractor independently. The voltage and current readings were confirmed with an external measurement to be accurate to within 2 % without calibration, which was considered sufficient for this work.

Thruster steady-state firing was performed with a constant voltage square wave with polarity alternating every 30 s. The alternation is necessary to avoid electrochemical reactions in the propellant [13] and the chosen period is sufficient with the large surface area carbon electrode [14]. The voltage setpoint was manually adjusted periodically to maintain the desired current output, which is nominally 150 µA. As an experiment, the second EMI-CF3BF3 thruster was operated at 250 µA current. Thruster startup and conditioning were performed in three steps. First, 300 V was applied for 3 min to activate the electrowetting valve, after which the thruster was left for several hours allow the propellant to flow to the emitter. Next, a square wave with 10 s polarity alternation was applied and the voltage was manually increased until emission of around 10 µA was seen, typically at 1000 V to 1400 V. This voltage was kept for a few minutes until a stable current over 30 µA was observed, after which the thruster was left again for several hours to soak. The final startup was performed with an 800 V square wave with 10 s alternation until the emitted current had stabilised. The voltage was then adjusted to reach nominal operation and the alternation period changed to 30 s after the current

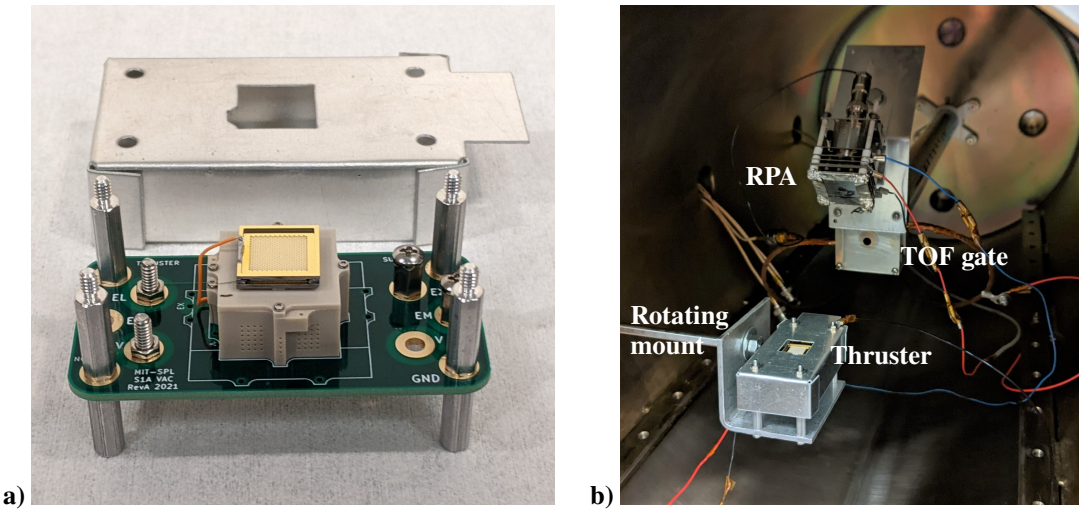

Fig. 4 a) Thruster mounted on test board with shield in background. b) Vacuum chamber diagnostics placement.

stabilised. The final startup sequence typically takes less than 10 min.

After the thrusters were started they were operated continuously in steady-state firing until the test ended, except when current v. voltage (IV) sweeps and RPA scans were performed. The IV-curve was captured using a triangle wave with a period of 60 s to a voltage which was estimated to give 300 µA maximum current. During RPA scans the thruster was operated in a single polarity for up to 60 s to allow time to gather sufficient data.

The propellant was outgassed in rough vacuum for at least 24 h before loading the thruster and the completed test assembly was weighed on an Adam Equipment AAA 250L scale with 0.2 mg repeatability before placing in the vacuum chamber. When the test finished the thruster was weighed again to determine the lost mass; presumed to represent the amount of propellant used. The output current was logged in all tests and the expelled charge was calculated by integrating the emitted minus intercepted current to calculate the true charge to mass ratio of the test.

B. Performance estimation

The thrust, specific impulse, and overall power efficiency were indirectly determined by measuring the ion beam and input power. We define efficiency as the jet power over electrical power[a]:

$$\eta = \frac{\dot{m}c^2}{2\mathbb{P}} = \frac{Fc}{2\mathbb{P}} = \frac{F^2}{2\dot{m}\mathbb{P}} \tag{1}$$

where $F = \dot{m}c$ was used to produce these equivalent expressions and $\mathbb{P} = V_0 I_{em}$. Several parameters impact the efficiency of the thruster, which can be separated as $\eta = \eta_i \eta_{tr}^2 \eta_\theta \eta_E \eta_p$ [15] from the contributions listed in Table 2. In this work, we assume $\eta_i = 1$ and show that $\eta_E > .99$ and $\eta_{tr} > .99$ for the tested thrusters. We thus take $\eta = \eta_p \eta_\theta$ and neglect the other terms to simplify the analysis.

Table 2 Sources of efficiency loss in electrospray thrusters [15].

Symbol	Name	Explanation
η_i	Ionisation	Fraction of propellant which leaves the thruster ionised
η_{tr}	Transmission	Fraction of extracted propellant which leaves the thruster
η_θ	Angular	Power lost due to the beam spreading out sideways
η_E	Energy	Power lost to liberate charged particles from the propellant
η_p	Polydispersive	Power lost due to differing mass of accelerated particles

The angular efficiency was estimated by assuming an axisymmetric current distribution and calculating the axial

[a]Specific impulse is defined by $I_{sp} = c/g$.

component of thrust (assumed to be proportional to current) by integrating the hemisphere [5]:

$$\eta_\theta = \left(\frac{\int_{-\pi/2}^{\pi/2} I(\theta) \cos(\theta) \sin(|\theta|)\, d\theta}{\int_{-\pi/2}^{\pi/2} I(\theta) \sin(|\theta|)\, d\theta} \right)^2 \tag{2}$$

where the contribution is squared since efficiency is proportional to thrust squared. $I(\theta)$ is measured from a full sweep of $-90°$ to $90°$, thus we introduce the absolute value in the sine function to integrate the whole dataset. The data was centred by subtracting the mean angle weighted by current before performing the integral.

The TOF measurement provides the polydispersive efficiency directly and thrust and specific impulse along the firing axis only, see Section IV.D. These must be corrected for the angular divergence to give the overall performance:

$$F = \sqrt{\eta_\theta}\, F_{TOF} \tag{3}$$

$$I_{sp} = \sqrt{\eta_\theta}\, I_{sp,TOF} \tag{4}$$

The amount of propellant used and charge expelled in a test can be used to calculate the specific impulse an ideal, lossless, electrospray thruster would generate at a given voltage [14]:

$$I_{sp}^{ideal} = \frac{1}{g}\sqrt{2V_0 \frac{q}{m}} \tag{5}$$

C. Vacuum chamber and diagnostics

All tests were conducted in a $\varnothing 40 \times 80$ cm cylindrical vacuum chamber in the MIT Space Propulsion Laboratory, depicted in Fig. 5. The chamber was evacuated by two turbomolecular pumps with a capacity of 45 L/s and 685 L/s respectively, operating in parallel and backed by a dry mechanical pump. The chamber pressure was monitored throughout testing and remained below 1 mPa for all experiments. The thrusters were mounted to a rotational mount with a precision rotary encoder so that the plume could be pointed at the diagnostic instruments within the chamber and the angular distribution could be measured.

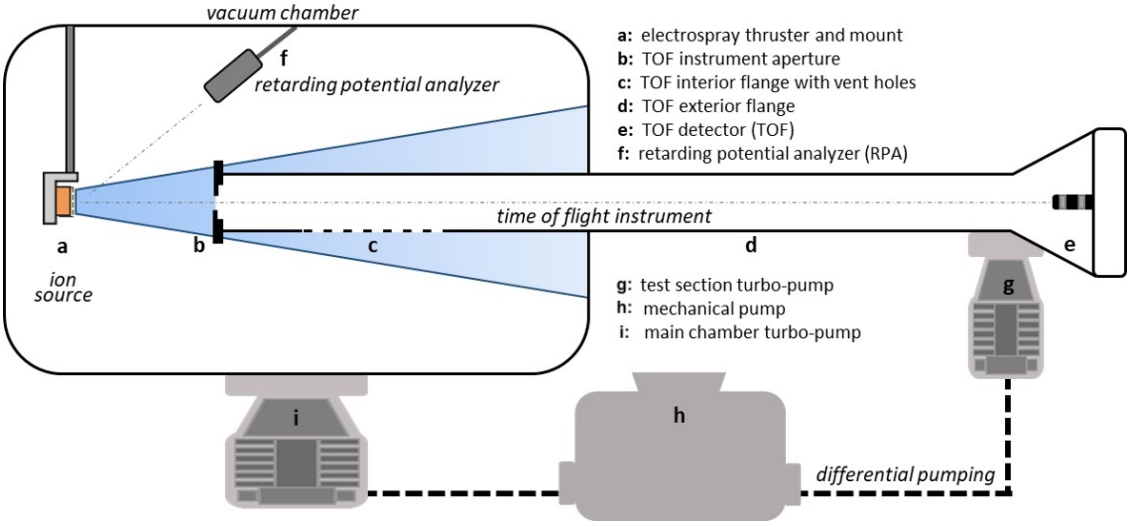

Fig. 5 Diagram of the vacuum chamber and diagnostic equipment used for thruster testing and performance characterisation.

In the initial test configuration, the rotational mount was attached at the top of the chamber (i.e. rotating about the vertical axis) such that the thruster beam was always horizontal. Due to the failure of the first test (see Section V.A) the chamber was reoriented to have the rotational mount at the side such that the thruster could be rotated into a vertical position for long duration firing. This was done since it is known that a thruster mounted to a filled propellant tank is affected by a gravity-induced pressure across the emitter array. Over time this can cause an ionic liquid short between

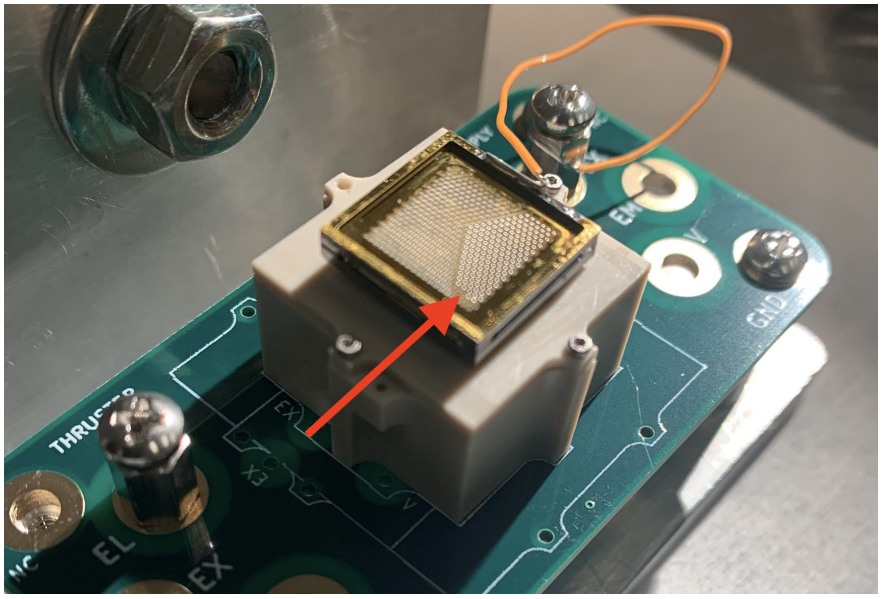

Fig. 6 Example of a partially flooded thruster due to sitting horizontally for several hours.

the thruster emitter and extractor at the bottom of the array; an example of how this may look is shown in Fig. 6. The second mount configuration is shown in Fig. 4b.

The retarding potential analyser (RPA) is one of two key diagnostic instruments installed in the chamber facility. The RPA used in this work consists of several high-transparency grids placed in front of a Faraday cup current collector. This is shown schematically in Fig. 7. The first grid is grounded, the second set of grids (RPA grids) are biased to some repelling potential V_{RPA}, then follows a second grounded grid, and the final grid is biased to −30 V to suppress secondary electron emission from the current collector. The RPA has a ⌀5 mm grounded aperture and is located approximately 15 cm downstream from the thruster.

To collect RPA measurements, the thruster is rotated into alignment with the RPA aperture and fired at a constant voltage. The repelling voltage V_{RPA} is set to a triangular voltage waveform between 0 V and a voltage higher in magnitude than the firing voltage. V_{RPA} and the current collected by the Faraday cup are controlled and measured using the same power supply and current-sensing circuitry as described in Section IV.A. Additionally, the RPA with all grids grounded acts as a current collector. This was used to measure the angular current distribution by firing the thruster in steady-state and sweeping it from −90° to 90° relative to the RPA. The RPA energy spectra and angular current distributions were recorded in both firing modes at each operating point.

D. Time-of-flight mass spectrometry

A mass spectra of the thruster plume was captured using a custom-built time-of-flight (TOF) mass spectrometer. A schematic of the TOF setup is shown in Fig. 8. The TOF instrument works by periodically interrupting the thruster's ion beam via an electrostatic deflection gate (also shown in Fig. 4b) approximately 16 cm away from the thruster, and measuring the drop-off of current on a downstream detector. The deflection gate consists of two rectangular electrodes pulsed at ±950 V a DEI PVM-2410 pulse amplifier. When the gate is open, ions will travel through a field-free region to a detector. The time for the ions to reach the detector depends on their charge-to-mass ratio (q/m), and is given by:

$$t_{TOF} = \frac{L_{TOF}}{\sqrt{2\left(\frac{q}{m}\right)V_0}} \tag{6}$$

where $L_{TOF} = 110$ cm. The detector is a Photonis Magnum 5900 Channel Electron Multiplier (CEM) which has a gain dependent on its bias voltage. For all tests, the CEM bias was set to 1.3 kV to 1.5 kV, which translates to a gain of $\approx 10^5$. Additionally, the front of the CEM detector was held at a high voltage with opposite polarity to the beam under test to ensure high-efficiency detection of all ions impacting the detector. The output of the CEM was further amplified by a factor of 50 using a custom operational amplifier (rise time <30 ns) and recorded by a Keysight DOSX3024A digital

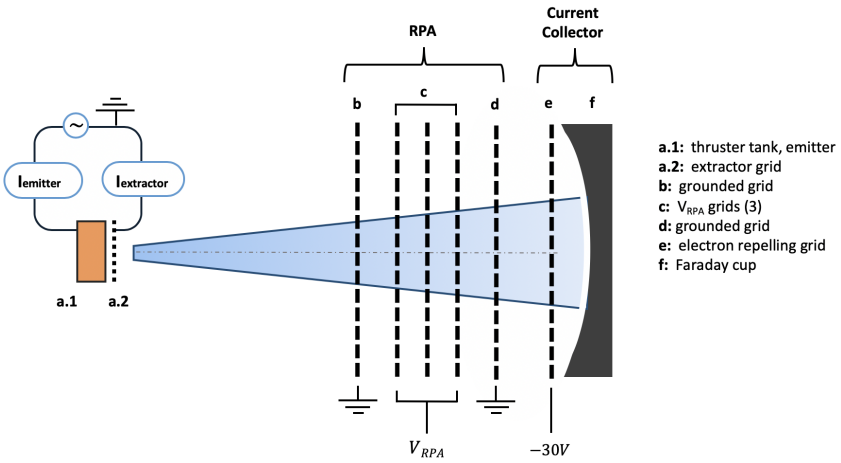

Fig. 7 RPA diagram

oscilloscope. The TOF gate was pulsed at 100 Hz and the signal was saved at the oscilloscope. In the positive firing mode, the signal was averaged 1024 times on the oscilloscope before saving. In the negative mode, due to experimental constraints, the data was averaged manually; 10 single scans of the signal were saved from the oscilloscope and then filtered, averaged, and smoothed in post-processing.

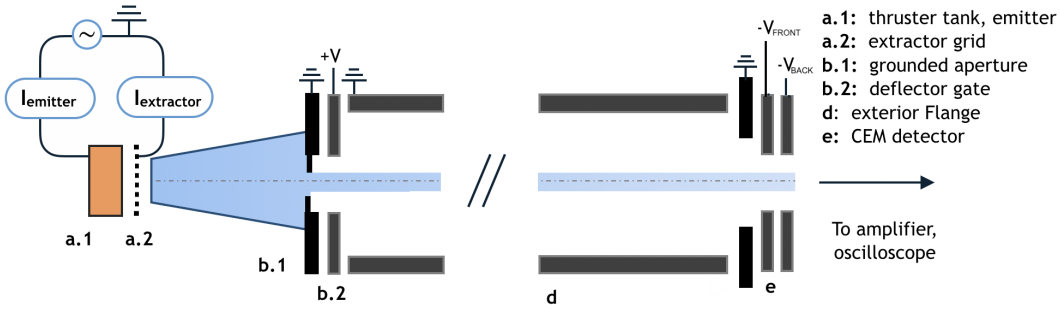

Fig. 8 Schematic of the time-of-flight (TOF) instrument used in this work. The voltage bias across the CEM is given by $V_{FRONT} - V_{BACK}$ and was always positive to attract the electron cascade.

The TOF signal was used to estimate thrust and mass flow rate from the detected ions, by integrating $I(t)$, the normalised current trace multiplied by the net emitted current I_{em} [16]:

$$F_{TOF} = \frac{2V_0}{L_{TOF}} \int_0^\infty I(t)\, dt \tag{7}$$

$$\dot{m}_{TOF} = \frac{4V_0}{L_{TOF}^2} \int_0^\infty tI(t)\, dt \tag{8}$$

This was used to estimate the specific impulse and polydisperive efficiency of the beam as:

$$I_{sp,TOF} = \frac{F_{TOF}}{g\dot{m}_{TOF}} \tag{9}$$

$$\eta_p = \frac{F_{TOF}^2}{2\dot{m}_{TOF} V_0 I_{em}} \tag{10}$$

Note that these calculations are taken only from the portion of the beam firing into the TOF instrument, which is along the thruster centreline for all tests. Additionally, these estimates do not account for contributions from neutral species.

E. Hygroscopy testing

To characterise the hygroscopic characteristics of potential propellants, different ionic liquids were subjected to increased relative humidity over long periods of time. The experimental setup comprised of a self-assembled humidity chamber with a piezo-activated humidifier that was commanded by a humidity sensor placed next to the samples. A closed loop electrical heater was used to stabilise the chamber temperature. The relative humidity and temperature control setpoint and accuracy were estimated to (80 ± 8) % and (30 ± 5) °C respectively. Different ionic liquids were placed in open 4 cm^3 vials, with an open surface area of 1.3 cm^2. An approximate sample volume of 1.2 cm^3 to 1.4 cm^3 was chosen, corresponding to sample weights ranging from approximately 0.6 g to 2.1 g. Initial weight measurement of the empty vials, as well as the filled vials after outgassing in a rough vacuum (<500 Pa) were used to establish the base ionic liquid mass. The samples were placed into the humidity chamber with provisions to prevent condensation from entering the openings of the sample vials. Periodic weight measurements after indicated storage times in the humidity chamber were performed directly after retrieval from the humidity chamber. All weight measurements were taken on an Adam Equipment AAA 250L scale with 0.2 mg repeatability.

Two additional tests were performed for the EMI-BF4 sample: After 37 days, the sample was removed from the humidity chamber and stored in the ambient laboratory atmosphere while continuing to perform periodic weight measurements. This test was used to verify the expected decrease in absorbed water by storage in a lower humidity, albeit uncontrolled, environment. In a second test, an EMI-BF4 sample with an increased ratio of surface area to liquid volume representative of the thruster's porous tank was placed in the same humidity chamber to observe how this affected the mass change rate.

V. Results

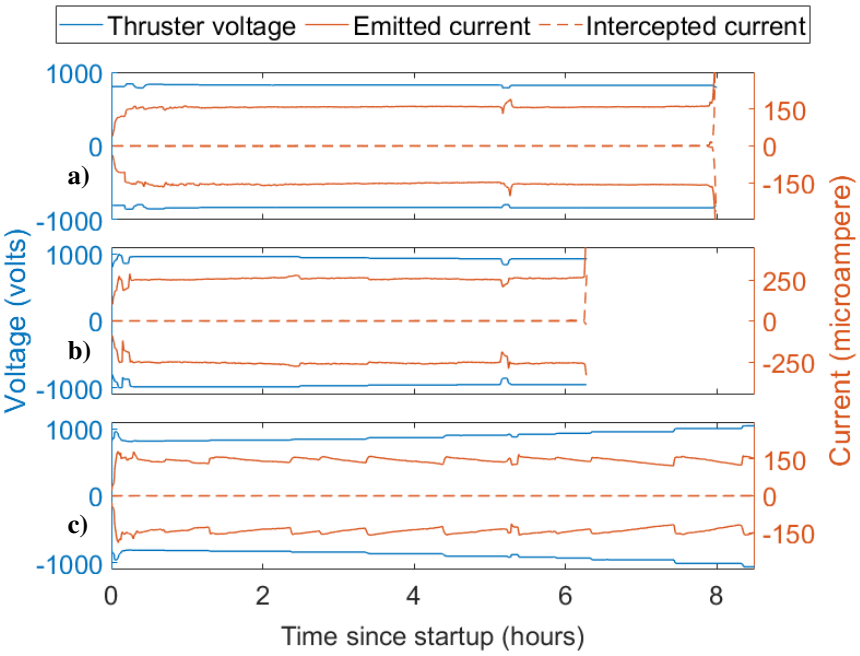

Fig. 9 Long-time thruster voltage and currents. The inconsistencies at the start and at five hours is during performance testing. a) First EMI-CF3BF3 thruster. b) Second EMI-CF3BF3 thruster. c) EMI-BF4 thruster.

A. Thruster operations

The first thruster tested used EMI-CF3BF3 propellant and was operated at the nominal 150 µA current, firing horizontally. The thruster started and operated normally for eight hours before it suddenly shorted, shown in Fig. 9a. The median intercepted current was 0.5 % and 0.4 % in positive and negative modes respectively. This test consumed 83.2 mg of propellant and emitted 2.183 C of positive charge and 2.142 C of negative charge, for a total average charge to mass ratio of 52.0 C/g. With a median operating voltage of 826 V and −832 V in the two polarities, the ideal specific impulse is 945 s and 948 s respectively. The thruster was inspected afterwards and was found to have propellant which had leaked onto the top of the tank, see Fig. 10a. This thruster was operated horizontally; we have experience with thrusters flooding after several hours in this orientation when mounted on a fuelled tank, but not when firing continuously. To mitigate the presumed failure mode the chamber was reconfigured to operate the following thrusters vertically as described in Section IV.C.

The second thruster used EMI-CF3BF3 propellant and was operated at 250 µA, where the higher current was chosen as an experiment since the previous thruster appeared to operate well at this current. After operating normally for six hours this thruster also shorted suddenly, shown in Fig. 9b. The median intercepted current was 0.3 % and 0.4 % in positive and negative modes respectively. In this test 2.814 C positive and 2.802 C negative charge was emitted while consuming 99.3 mg of propellant. This gives an average charge to mass ratio of 56.6 C/g and an ideal specific impulse of 1048 s and 1061 s respectively for the median positive and negative voltages applied of 933 V and −957 V. After inspection, we again observed propellant leaking onto the top of the tank, see Fig. 10b. As this thruster failed in a similar manner to the previous one it was determined that the orientation was not the likely cause of the two failures. Instead, an insufficient seal between the thruster chip frame and tank/valve cap is the presumed cause. For these two thrusters this seal was created solely by the proximity of mating surfaces, which is evidently insufficient. The future thrusters have this interface sealed with epoxy during assembly, guaranteeing containment, but making disassembly and reuse difficult.

The third thruster used EMI-BF4 as propellant and was operated at the nominal current of 150 µA. This thruster was fired vertically and operated for a total of 27 h before the test was ended with a still-functional thruster. The median intercepted current was 0.4 % and 0.1 % in positive and negative modes respectively. This thruster showed fast current decay during operations, and thus the voltage was increased to compensate, seen in Fig. 9c. This behaviour is unusual

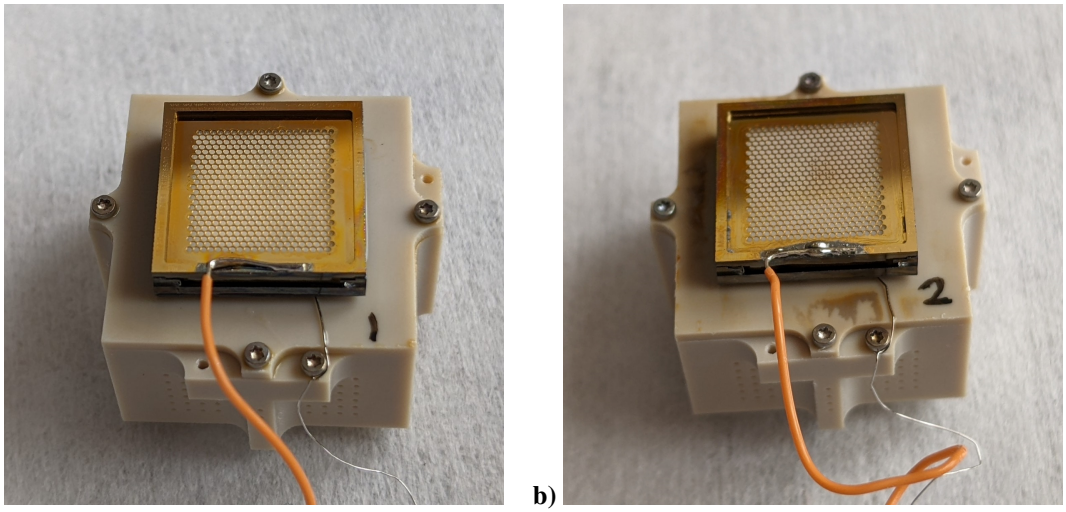

Fig. 10 Leaks between tank and thruster frame. a) On the first thruster a liquid meniscus is evident around the screw heads and valve wire. b) On the second thruster ionic liquid has discoloured the tank cap.

for a thruster with a tank, which typically operates with stable current until propellant starts to deplete [17, see Fig. 10]. The decay was likely caused by inadvertently creating a restriction in the tank during assembly, possibly by liberally applying epoxy to seal the tank-frame interface. This test confirmed that the leaks seen in the previous thrusters was mitigated, and was stopped after 25 h when the voltage required for nominal emission was 1.7 kV and −1.8 kV in the two modes, over twice the startup voltage. After resting the thruster for 24 h it was restarted and again required a typical voltage to reach nominal current, but thent decayed to half of this current in less than two hours. The normal restart and subsequent decay confirmed that a propellant flow restriction was the likely cause of the observed behaviour. This test consumed 81.0 mg of propellant while emitting 6.101 C and 6.020 C of positive and negative charge respectively for a charge to mass ratio of 150 C/g. This ratio suggests that the ideal specific impulse of this test was relatively high, however due to the varying voltage we can not calculate it here.

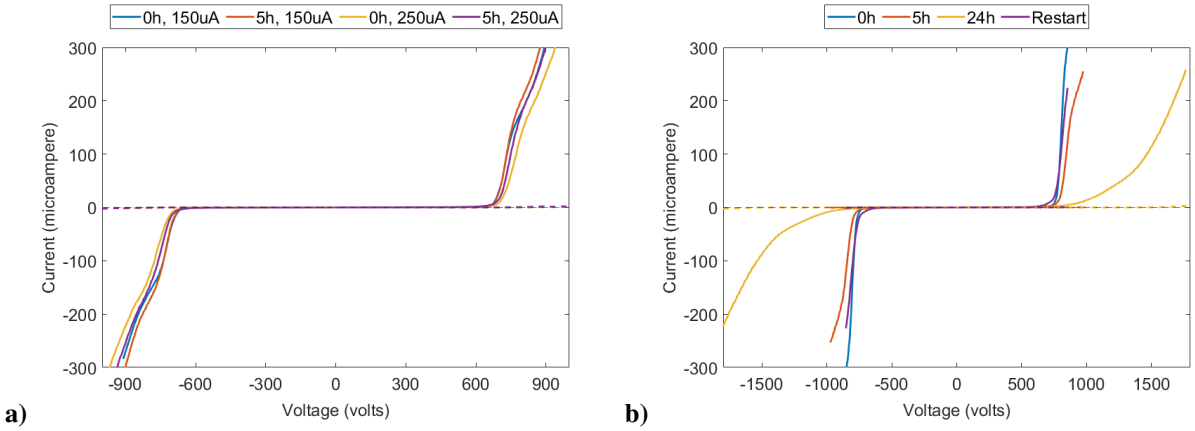

Fig. 11 IV curve for the thrusters at different test duration. The emitted current is solid and the intercepted current is dashed. a) The two EMI-CF3BF3 thrusters. b) The EMI-BF4 thruster.

B. EMI-CF3BF3 performance testing

The two EMI-CF3BF3 thrusters had a startup voltage of approximately ±670 V and show similar IV characteristics during initial startup and after five hours operation, shown in Fig. 11a. These data show that the intercepted current is small, <1 %, and therefore $\eta_{tr} > .99$ for all tests performed. The suite of performance testing was performed at startup

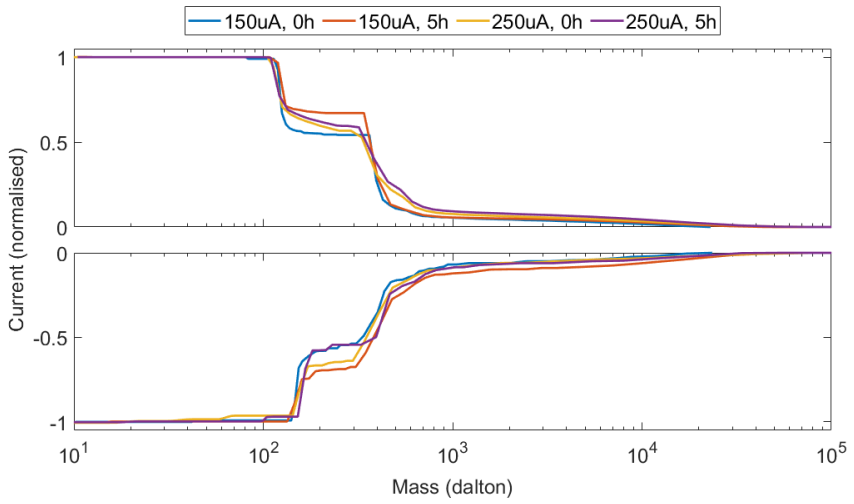

Fig. 12 TOF traces for both EMI-CF3BF3 thrusters operating in positive and negative polarity.

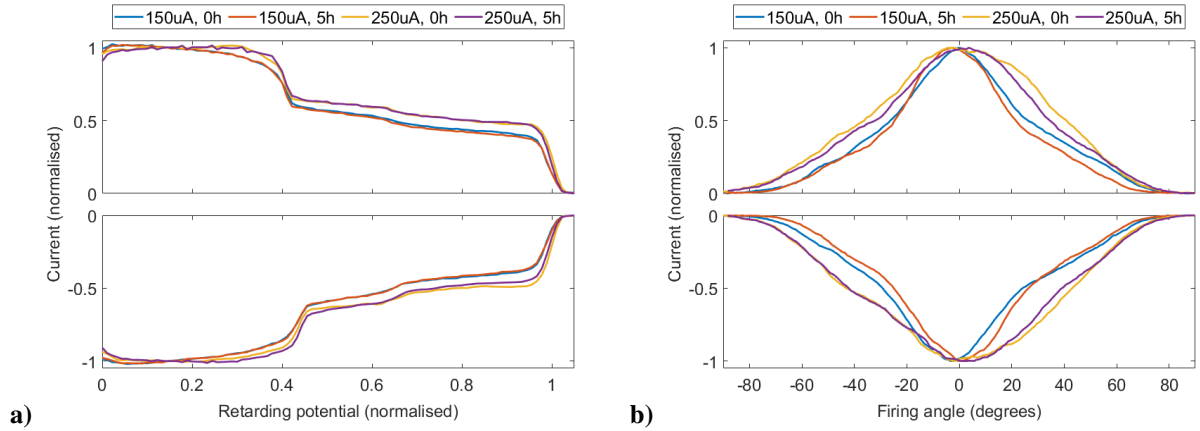

Fig. 13 Data for both EMI-CF3BF3 thrusters operating in positive and negative polarity. a) Energy spectrum from RPA. b) Angular current distribution.

Table 3 Performance data for the two thrusters tested with EMI-CF3BF3 propellant.

Experiment	V_0 (V)	I_{em} (µA)	$\mathbb{P}$ (mW)	F_{TOF} (µN)	$I_{sp,TOF}$ (s)	η_p	η_θ	F (µN)	I_{sp} (s)	η
0 h, 150 µA	836	150	125	12.2	1166	56%	62%	9.6	917	35%
	-852	-150	128	13.5	1072	56%	62%	10.6	843	34%
5 h, 150 µA	821	150	123	13.6	897	49%	65%	11.1	725	32%
	-837	-150	126	17.9	594	42%	66%	14.5	481	27%
0 h, 250 µA	959	250	240	25.8	758	40%	58%	19.7	578	23%
	-983	-250	246	27.0	782	42%	58%	20.6	597	24%
5 h, 250 µA	927	250	232	27.4	692	40%	58%	20.8	526	23%
	-951	-250	238	26.8	835	46%	58%	20.3	634	27%

Note: The 0 h, 150 µA TOF truncated the higher mass particles and thus shows an artificially low thrust and high specific impulse.

and after five hours.

The TOF results are shown in Fig. 12 and Table 3. The uncorrected TOF results show a thrust around 13 μN with a specific impulse around 900 s at 130 mW input power for the nominal 150 μA case. The thruster operated at 250 μA produces a thrust around 27 μN, specific impulse around 700 s, and requires 240 mW power. The polydispersive efficiency is around 45 % and appears marginally higher at the nominal current. These results show a droplet population of 5 % to 12 % which increases the thrust but degrades the efficiency and specific impulse compared to pure ion emission.

The RPA results are shown in Fig. 13a, where the rightmost step in the curve occurs when the retarding potential is equal to the firing voltage, thus unfragmented species in the beam arrive with negligible energy loss and therefore $\eta_E > .99$. The middle step in the RPA shows that around 40 % of the beam are dimers which have fragmented into monomers outside the acceleration region, consistent with the TOF results.

The angular current distribution is shown in Fig. 13b, where the full width at half maximum (FWHM) angle is approximately 50° in both modes at 150 μA, and 70° and 80° at the higher current in positive and negative modes respectively. Note that these two samples were operated horizontally and vertically respectively, so the results may be affected by the change in gravity vector. The calculated angular efficiency, given in Table 3, is on average 64 % and 58 % for the two thrusters, corresponding to a reduction in thrust and specific impulse of 20 % and 24 % respectively.

C. EMI-BF4 performance testing

The thruster with EMI-BF4 propellant required a voltage of approximately ±740 V to start up, as shown in Fig. 11b. After five hours of operation the IV-curve was degraded by around 60 V, and at 24 h the voltage required was doubled, owing to the propellant flow restriction discussed in Section V.A. In all cases the intercepted current was <1 % and therefore $\eta_{tr} > .99$. The suite of performance testing was performed at startup, after five hours, after 24 h, and after the thruster had been turned off for 24 h to allow propellant to flow to the emitter. As seen in Fig. 11b, the original IV-curve was largely recovered by this, however with a less sharp startup voltage.

The TOF trace and derived performance are shown in Fig. 14 and Table 4. The uncorrected TOF results show a thrust of approximately 14 μN with a specific impulse around 700 s at 120 mW input power for the initial startup. After five hours the thrust was similar at 13 μN, with an improved specific impulse around 1000 s while requiring 140 mW. The droplet population is 3 % to 10 % of the beam which is fewer than the EMI-CF3BF4 results, however, the droplets are larger and the specific impulse is thus lower. After 24 h, when the thruster was operated away from nominal condition, the specific impulse was similar, but the thrust had increased to 18 mN at an input power of 150 mW. After restarting the thruster following a period of rest, the positive mode TOF results were comparable to the original results. Notably however, the negative mode showed that the thruster was now operating in the pure ion evaporation mode with an undetectable presence of droplets. In this mode, a thrust of approximately 8 μN was produced with a specific impulse of 3000 s, requiring 240 mW of power and delivering a polydispersive efficiency above 90 %.

The RPA results for EMI-BF4 are shown in Fig. 15a. Here the rightmost step is also at the full firing potential and therefore $\eta_E > .99$. We notice some evidence of fragmentation in the acceleration region for this propellant which was not observed in the previous testing, however this appears to reduce over time.

The angular current distribution is shown in Fig. 15b, where the FWHM angle is approximately 60° with an efficiency of 69 % in both modes at the initial measurement (i.e. the thrust and specific impulse are degraded by 17 %), which is slightly worse than the EMI-CF3BF3 results. After five hours and after the restart this had increased to 80° FWHM with an efficiency around 60 %. The angular distribution after 24 h is clearly bimodal; the current is output in a ring around the normal firing axis. The high voltage required to reach nominal current at this stage may have caused the the individual emission sites to bifurcate into two or more sites each, spraying significantly off-axis. This behaviour has been observed at high voltages for both cone-jet [18] and pure ion evaporation [19] single-emitter electrosprays.

D. Propellant performance comparison

In Table 5 the performance for each propellant has been averaged across both polarities to produce a final estimate. For the EMI-CF3BF3 data at nominal current, the 5 h test was used since the initial data was affected by truncated TOF. For EMI-BF4 the 0 h test was used because of the tank flow restriction. EMI-CF3BF3 at 250 μA was included for reference and is the average of the 0 h and 5 h data. This shows that the overall performance is similar between the two propellants, with EMI-CF3BF3 producing marginally higher thrust, specific impulse, and efficiency. When operating at the higher current the specific impulse and efficiency are degraded, but a higher thrust is generated as expected.

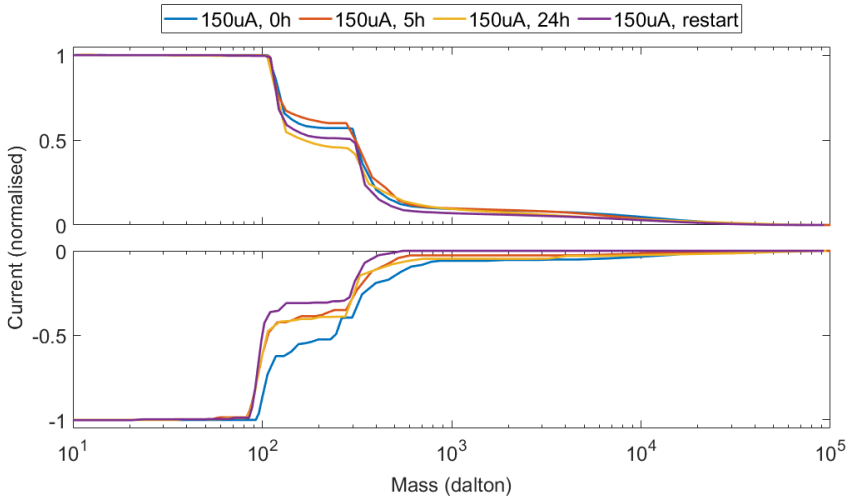

Fig. 14 TOF traces for the EMI-BF4 thruster in positive and negative polarity.

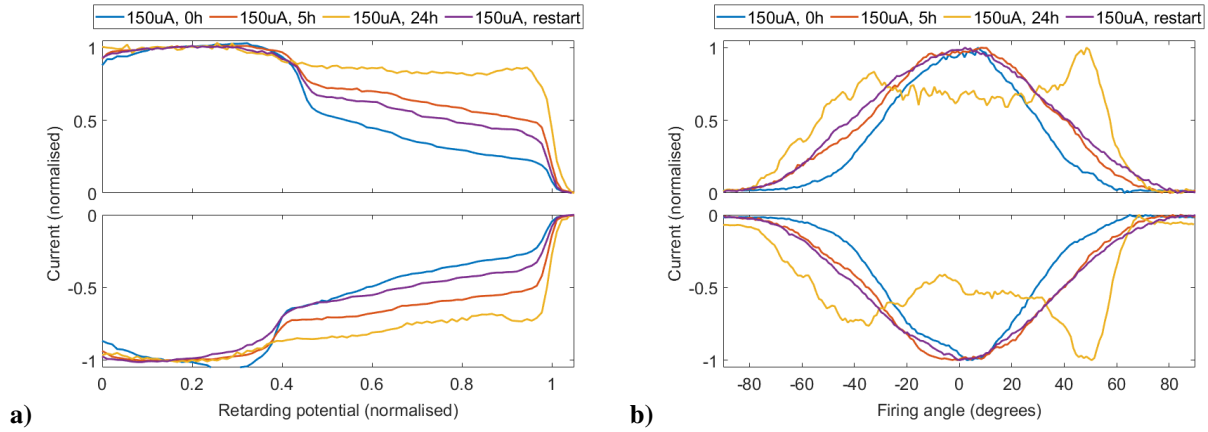

Fig. 15 Data for the EMI-BF4 thruster operating in positive and negative polarity. a) Energy spectrum from RPA. b) Angular current distribution.

Table 4 Performance data for the thruster tested with EMI-BF4 propellant.

Experiment	V_0 (V)	I_{em} (µA)	$\mathbb{P}$ (mW)	F_{TOF} (µN)	$I_{sp,TOF}$ (s)	η_p	η_θ	F (µN)	I_{sp} (s)	η
0 h	816	150	122	14.9	649	39%	69%	12.3	538	27%
	-812	-150	122	12.7	758	39%	69%	10.6	629	27%
5 h	919	150	138	15.7	724	41%	60%	12.2	562	24%
	-915	-150	137	10.4	1196	44%	61%	8.1	938	27%
24 h	1616	150	242	19.3	930	36%	51%	13.8	663	19%
	-1713	-150	257	16.7	883	28%	46%	11.3	599	13%
Restarted	842	150	126	13.0	815	41%	58%	9.9	619	24%
	-838	-150	238	7.8	3000	91%	59%	6.0	2300	53%

Table 5 Averaged performance data for the thrusters tested with different propellants.

Propellant	Current (µA)	Power (mW)	F (µN)	I_{sp} (s)	η
EMI-CF3BF3	±150	124	12.7	603	30%
EMI-BF4	±150	122	11.5	583	27%
EMI-CF3BF3	±250	239	20.4	584	24%

E. Hygroscopy testing

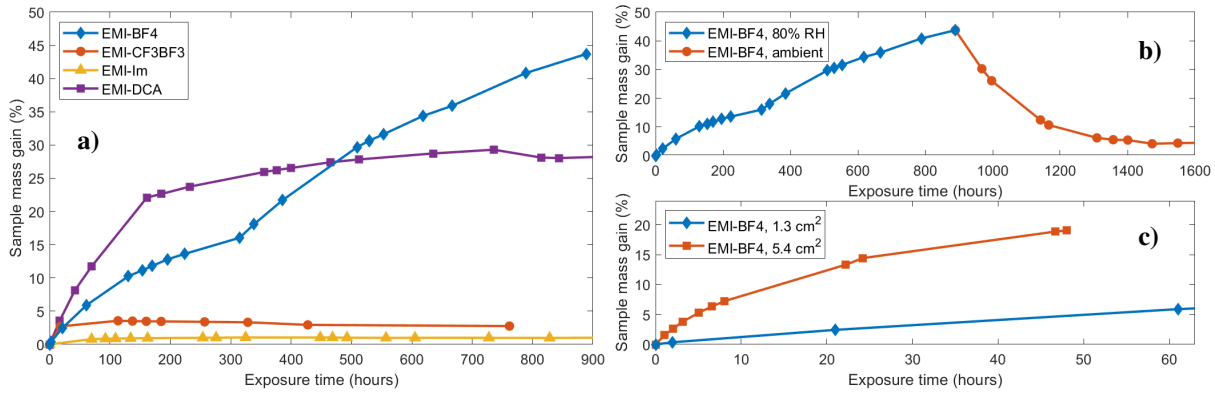

Fig. 16 a) Weight increase of different ionic liquid samples during storage in 80% RH environment, relative to the outgassed initial weight. b) Decrease of EMI-BF4 sample weight after removal from high humidity environment. c) Comparison of EMI-BF4 absorption rate for increased contact surface are area.

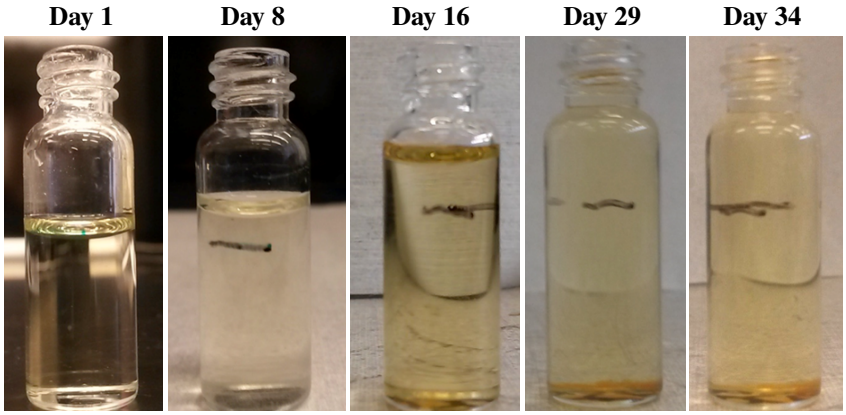

Fig. 17 Volume increase of EMI-BF4 sample after prolonged storage at 80% RH.

The four candidate ionic liquids EMI-BF4, EMI-CF3BF3, EMI-Im, and EMI-DCA were tested in the humidity chamber for approximately one month each, with their mass gain shown in Fig. 16a. Despite the limited accuracy of the experimental setup, significant humidity intake for certain ionic liquids is evident, including the canonical EMI-BF4. The significant volume increase of EMI-BF4 is apparent in Fig. 17. EMI-DCA experiences relatively fast humidity intake, but was found to saturate below 30% mass increase. The other ionic liquids, EMI-Im and EMI-CF3BF3, showed a saturated sample mass increase below 5%. High relative mass increase, and associated volume increase, can pose an issue for propellant storage and integration in an uncontrolled environment. To account for this, a controlled environment from propellant loading to reaching space, using a sealed tank, or including significant unused tank volume is required.

The mass loss of the EMI-BF4 sample is shown in Fig. 16b after it was removed from the humidity chamber. This verified that the absorbed water will leave the propellant in a lower humidity environment, until a new equilibrium is reached. Fig. 16c shows the mass gain of EMI-BF4 repeated with a larger surface area, representative for a porous tank. It is clear that this accelerates the absorption, and that 24 h at 80% RH is sufficient to absorb almost 15% water mass.

VI. Conclusions

In this work we tested the three first units of the new iEPS thruster generation for the STEP-1 mission. Perhaps expectedly, there were some issues with these thrusters as the team refines the assembly procedure. The new thruster appears to operate well, and shows especially an exceptionally low intercepted current. This could be one step towards longer lifetime operation of electrosprays than previously attained. We observed an unexpectedly wide beam divergence, and this may be related to the new extractor as well, where the apertures have become so wide that the electric fields

may start to "leak" significantly.

Comparing the two propellants tested in detail, EMI-BF4 and EMI-CF3BF3, the results are very promising. The performance characterisation show that there is little difference between the selection in the tested configuration, where if anything the new option of EMI-CF3BF3 performs better. Simultaneously we show that this propellant does not absorb water, whereas EMI-BF4 takes on water at a troublesome rate. Therefore, STEP-1 is likely to proceed with EMI-CF3BF3.

The ultimate performance numbers attained here are similar to that seen in previous generations of iEPS thrusters, e.g. [14]. This may be less than ideal, but the new materials and design changes leave headroom to adjust the thruster from this starting point. One of our tests showed the thruster enter into a true pure-ion evaporation mode, which could indicate that only small tweaks are necessary.

Finally, to help further the use of ionic liquids in electrosprays and elsewhere, it would be useful to map the equilibrium absorbed water fraction of popular ionic liquids as a function of temperature and humidity. With this knowledge, designing tanks with appropriate excess volume and determining the environmental and handling requirements of ionic liquids would be aided considerably.

Acknowledgements

Support of this work was provided by the NASA Small Satellite Technology Partnership Program and other U.S. Government agencies. The authors thank Saba Shaik for helping reorient the vacuum chamber.

References

[1] Huberman, M. N., Beynon, J. C., Cohen, E., Goldin, D. S., Kidd, P. W., and Zafran, S., "Present status of colloid microthruster technology," *Journal of Spacecraft and Rockets*, Vol. 5, No. 11, 1968, pp. 1319–1324. https://doi.org/10.2514/3.29476.

[2] Romero-Sanz, I., Bocanegra, R., Fernandez de la Mora, J., and Gamero-Castaño, M., "Source of heavy molecular ions based on Taylor cones of ionic liquids operating in the pure ion evaporation regime," *Journal of Applied Physics*, Vol. 94, No. 5, 2003. https://doi.org/10.1063/1.1598281.

[3] Krecji, D., et al., "Full Performance Mapping of the IFM Nano Thruster, Including Direct Thrust Measurements," *Journal of Small Satellites*, Vol. 8, No. 2, 2019, pp. 881–893.

[4] Tsay, M., Model, J., Barcroft, C., Frongillo, J., Zwahlen, J., and Feng, C., "Integrated Testing of Iodine BIT-3 RF Ion Propulsion System for 6U CubeSat Applications," *Proceedings of the 35th International Electric Propulsion Conference*, Atlanta, Georgia, 2017.

[5] Petro, E. M., Bruno, A. R., Lozano, P. C., Perna, L. E., and Freeman, D. S., "Characterization of the TILE Electrospray Emitters," *Proceedings of the AIAA Propulsion and Energy Forum*, Virtual Event, 2020. https://doi.org/10.2514/6.2020-3612.

[6] Ziemer, J., and Merkowitz, S., "Microthrust propulsion for the LISA mission," *40th AIAA/ASME/SAE/ASEE Joint Propulsion Conference and Exhibit*, 2004, p. 3439.

[7] Cuadrado-Prado, S., Domínguez-Pérez, M., Rilo, E., García-Garabal, S., Segade, L., Franjo, C., and Cabeza, O., "Experimental measurement of the hygroscopic grade on eight imidazolium based ionic liquids," *Fluid Phase Equilibria*, Vol. 278, No. 1, 2009. https://doi.org/10.1016/j.fluid.2008.12.008.

[8] Ohtsuki, J., Matsumoto, K., and Hagiwara, R., "Physical and electrochemical properties of 1-ethyl-3-methylimidazolium ionic liquids of mixed anions,(FH) nF-, BF4-, and N (SO2CF3) 2-," *Electrochemistry*, Vol. 77, No. 8, 2009.

[9] Zhang, S., Lu, X., Zhou, Q., Li, X., Zhang, X., and Li, S., *Ionic Liquids: Physicochemical Properties*, Elsevier, Amsterdam, 2009. https://doi.org/10.1016/B978-0-444-53427-9.00002-6.

[10] MacArthur, J., Kristinsson, B. O., Freeman, D., Petro, E., Li, H., and Lozano, P. C., "Microfluidic and Extractor Electrode Update in the ion-Electrospray Propulsion System," *36th International Electric Propulsion Conference*, 2019.

[11] Brikner, N., and Lozano, P. C., "The role of upstream distal electrodes in mitigating electrochemical degradation of ionic liquid ion sources," *Applied Physics Letters*, Vol. 101, No. 19, 2012, p. 193504.

[12] Kristinsson, Ö., Freeman, D., Petro, E., Lozano, P. C., Hsu, A., Young, J. A., and Martel, F., "Operation and Performance of a Fully-Integrated ionic-Electrospray Propulsion System," *Proceedings of the 36th International Electric Propulsion Conference*, 2019.

[13] Lozano, P., and Martínez-Sánchez, M., "Ionic liquid ion sources: suppression of electrochemical reactions using voltage alternation," *Journal of Colloid and Interface Science*, Vol. 280, No. 1, 2004. https://doi.org/10.1016/j.jcis.2004.07.037.

[14] Krejci, D., Mier-Hicks, F., Thomas, R., Haag, T., and Lozano, P., "Emission Characteristics of Passively Fed Electrospray Microthrusters with Propellant Reservoirs," *Journal of Spacecraft and Rockets*, Vol. 54, No. 2, 2017. https://doi.org/10.2514/1.A33531.

[15] Lozano, P., and Martinez-Sanchez, M., *Efficiency Estimation of EMI-BF4 Ionic Liquid Electrospray Thrusters*, 2005. https://doi.org/10.2514/6.2005-4388.

[16] Gamero-Castano, M., and Hruby, V., "Electrospray as a Source of Nanoparticles for Efficient Colloid Thrusters," *Journal of Propulsion and Power*, Vol. 17, No. 5, 2001. https://doi.org/10.2514/2.5858.

[17] Krejci, D., and Lozano, P. C., "Micro-Machined Ionic Liquid Electrospray Thrusters for CubeSat Applications," *Proceedings of the 35th International Electric Propulsion Conference*, Atlanta, Georgia, 2017.

[18] Ryan, C., Smith, K., and Stark, J., "Characterization of multi-jet electrospray systems," *Journal of Aerosol Science*, Vol. 51, 2012. https://doi.org/10.1016/j.jaerosci.2012.03.007.

[19] Perez-Martinez, C. S., and Lozano, P. C., "Visualization of beams from ionic liquid ion sources for focused ion beam applications," *Journal of Vacuum Science & Technology B*, Vol. 30, No. 6, 2012. https://doi.org/10.1116/1.4745187.